Supporting Information

CO_2-actuated Spin Transition Tuning in an Interdigitated Hofmann-type Coordination Polymer

Abhik Paul,[a] Wataru Kosaka,[bc] Bhart Kumar,[a]† Dibya Jyoti Mondal,[a]† Hitoshi Miyasaka,*[bc] Sanjit Konar*[a]

[a]Molecular Magnetism Lab, Department of Chemistry, Indian Institute of Science Education and Research, Bhopal, Madhya Pradesh, India-462066. E-mail: skonar@iiserb.ac.in

[b]Institute for Materials Research, Tohoku University, 2-1-1 Katahira, Aoba-ku, Sendai 980-8577, Japan.

[c]Department of Chemistry, Graduate School of Science, Tohoku University, 6-3 Aramaki-Aza-Aoba, Aoba-ku, Sendai 980-8578, Japan. *E-mail: miyasaka@imr.tohoku.ac.jp*

†these authors contributed equally.

Table of contents for supplementary Information

Materials and Methods:

All chemicals and reagents were of analytical grade and were used as received from commercial sources. Framework 1 was obtained and characterised using a previously reported procedure.[1]

Synthesis of framework 1·1.3MeOH. A bulk crystalline sample of **1·1.3MeOH** was prepared by liquid-to-liquid slow diffusion technique. The ligand methyl isonicotinate (12 mg, 0.084 mmol) and $K_2[Pd(CN)_4].xH_2O$ (12.1 mg, 0.042 mmol) were taken in methanolic solution and placed on the top layer, and aqueous solution of $Fe(ClO_4)_2 \cdot 6H_2O$ (15.2 mg, 0.042 mmol) was placed in the bottom layer. The layering tubes were kept separately for crystallisation without any disturbance. Yellow hexagonal plate crystals of **1·1.3MeOH** formed in quantitative yield over 6 weeks. IR (solid, ν/cm−1) 3336.8 (br), 2167.4 (sh), 1634.4 (br), 1510.3 (w), 1433.3 (sh), 1383.8 (w), 1325.5 (w), 1288.4 (w), 1208.2 (w), 1170.8 (w), 1054.0 (sh), 998.6 (w), 960.7 (w). CHN calcd. (for $C_{20}H_{22}FeN_6O_6Pd$): C, 39.72; H, 3.67; N, 13.90. Found: C, 39.65; H, 3.61; N, 13.50.

Synthesis of framework 1. To obtain completely desolvated framework **1**, a bulk quantity of single crystals of **1·1.3MeOH** was taken in a vial and heated at 180 ºC under vacuum for 3 hours, according to TGA). The completion of the desolvation process was confirmed by IR spectroscopy and elemental analysis. IR (solid, ν/cm^{-1}) 3006.8 (w), 2167.8 (sh), 1636.4 (br), 1512.3 (br), 1380.7 (sh), 1322.7 (w), 1208.2 (w), 1170.8 (w), 1053.0 (sh), 996.6 (w), 962.7 (w). CHN calculated. (for $C_{18}H_{14}FeN_6O_4Pd$): C, 39.95; H, 2.68; N, 15.59; obtained: C, 39.60; H, 2.38; N, 15.30.

Synthesis of framework 1·CS_2. A bulk crystalline sample of **1·CS_2** was prepared by a similar liquid-to-liquid slow diffusion technique as **1·1.3MeOH**, using a methanolic solution of CS_2 as the buffer layer.

Physical Measurement:

Fourier Transform Infrared Spectroscopy. The FT-IR experiments were carried out using a Perkin Elmer spectrometer and attenuated total reflection (ATR) correction setup has been done between the range of 400–4000 cm^{-1}. To guarantee optimal optical contact, the powdered samples were squeezed between a diamond crystal and a bridge-clamped sapphire anvil. the peaks were assigned based on the reported literature.

Thermogravimetric Analysis. The thermal stability of the samples was analysed with a Perkin Elmer TGA-6000 thermobalance operating at a heating rate of 5 K min^{-1}, under dry N_2 atmosphere.

Powder XRD. Powder X-ray diffraction patterns of the samples (framework **1** and **1·1.3MeOH**) were obtained at 298 K on PANalytical Empyrean X-Ray Diffractometer with a Cu Kα radiation (λ=1.54060Å). The bulk powder of each sample was placed on a silica sample holder and measured by a continuous scan between 5–50º with a step size of 0.013103˚.

In-situ VT-PXRD. The ground sample was sealed in a soda-lime glass capillary with an inner diameter of 0.5 mm. The PXRD pattern was obtained in the range 5−50º with 0.05° steps using a Rigaku Ultima IV diffractometer with Cu Kα radiation (λ = 1.5418 Å). To obtain the PXRD patterns under gas-adsorbed conditions, the glass capillary was connected to stainless steel lines that possessed valves to dose and remove gas, which were connected to a gas-handling system (BELSORP MINI X, MicrotracBEL). Temperature dependence of PXRD patterns was collected under fixed gas pressure (100 kPa of He or 100, 32, 10, and 3.2 kPa of CO_2). The temperature was controlled using a stream of

N_2 gas. Unlike in-situ measurements in a SQUID, the lower limit of the measurement temperature is limited by the sublimation temperature of CO_2 since the formation of solid CO_2 breaks glass capillaries.

Single Crystal X-ray Diffraction (SCXRD) Single Crystal X-ray diffraction data were collected on Bruker D8 Venture diffractometer using monochromated Mo Kα radiation (λ = 0.71073 Å) at 100 K using an Oxford Cryostream low-temperature device. Unit cell measurements, data integration, scaling and absorption corrections for the crystals were done with Bruker APEX-3 software. Data reduction was carried out with Bruker SAINT suite. Absorption correction was performed by the multi-scan method implemented in SADABS. All the crystal structures were solved by direct methods using SIR 2014. The crystal structure refinements were done in the program package Olex2,[1] and all non-hydrogen atoms were refined anisotropically by full-matrix least-squares calculations based on F2 with SHELXL-2018.[2] Some hydrogen atoms were located from the difference Fourier Map, while the remaining hydrogen atoms were included in calculated positions as riding atoms. Details of crystal data, data collection, and refinement details are given in Table S3-S6.

Gas adsorption measurements. The sorption isotherm and isobar measurements for N_2, O_2, and CO_2 were carried out using an automatic volumetric adsorption apparatus (BELSORP MAX, MicrotracBEL) connected to a cryostat system (ULVAC-Cryo. A known weight (~40 mg) of **1** was placed into the sample cell, which was again evacuated before measurements for 12 h at 430 K. Then the change in pressure was monitored, and the degree of adsorption was determined based on the decrease in pressure at the equilibrium state. When the reading of the pressure gauge for 500 seconds was within 0.3%, the system was judged to have reached adsorption equilibrium.

Magnetic Susceptibility Measurements. Magnetic measurements of framework **1** were performed using a Quantum Design MPMS2 SQUID magnetometer equipped with a 7 T magnet, operating at 1000 Oe at the temperature range of 2−300 K. The measured values were corrected for the experimentally measured contribution of the sample holder, whereas the derived susceptibilities were corrected for the diamagnetic contribution of the sample, estimated from Pascal's tables.

Magnetic measurements under CO_2 atmosphere were performed using a home-built sealed gas cell.

CO_2 gas was filled at RT to each pressure, then M-T curves were measured in the range 300-10 K at 1000 Oe and sweep mode (0.5 K min^{-1}). For the measurement without CO_2 (CO_2 = 0 kPa) in a sealed cell, 100 kPa of He gas was introduced to enhance thermal conductivity instead of vacuum, followed by the measurement under different CO_2 pressure in the order of 100 kPa, 32 kPa, 10 kPa, 3.2 kPa, 1 kPa, and He (2^{nd}), to check the sample was reverted back to its original state.

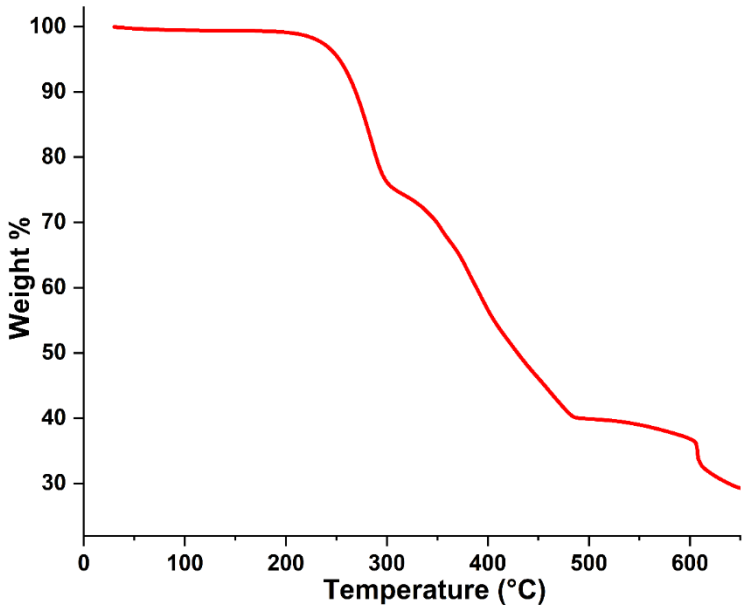

Figure S1. Thermogravimetric analysis of framework **1**.

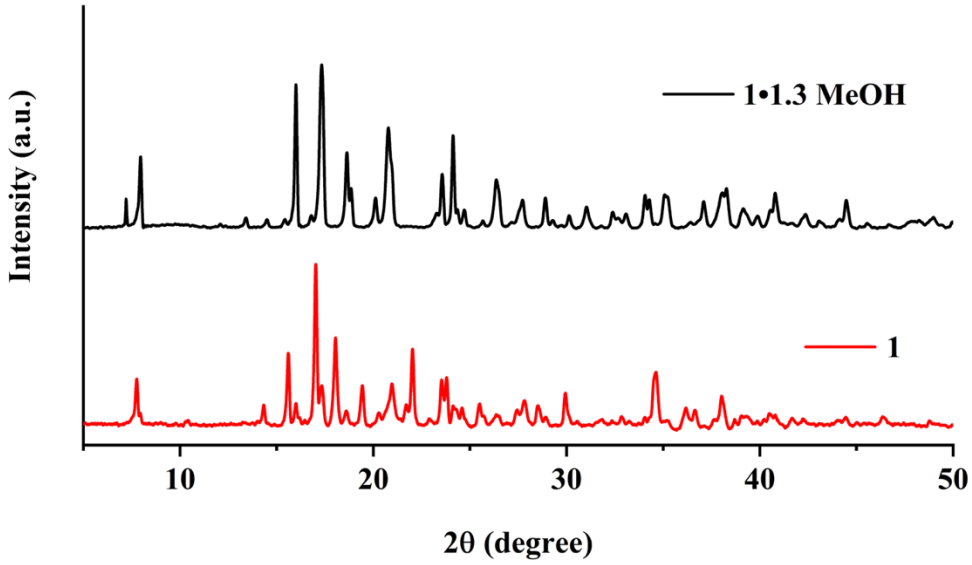

Figure S2. Comparative PXRD spectrum of the parent framework **1**·1.3MeOH (black) and **1** (red).

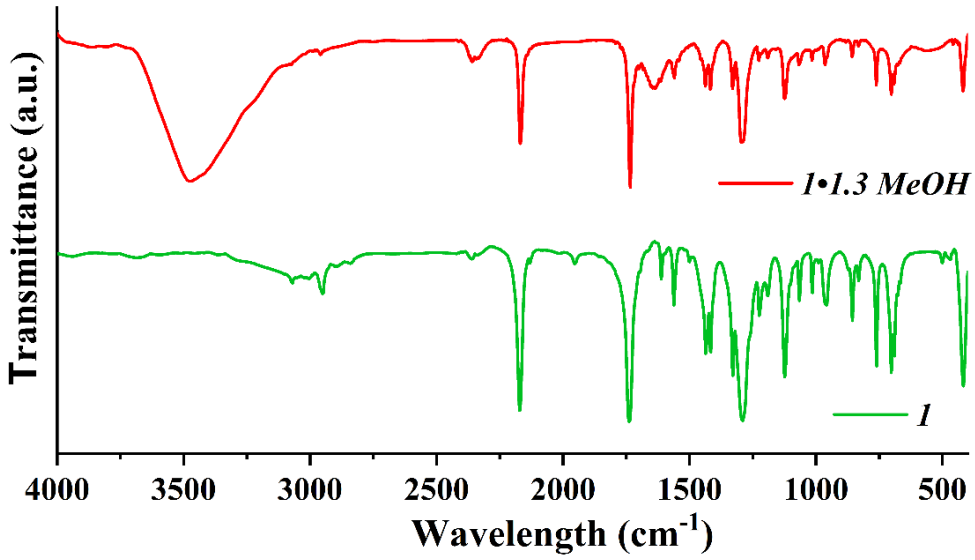

Figure S3. Comparative FTIR spectra of framework **1**·1.3MeOH (red) and framework **1** (green).

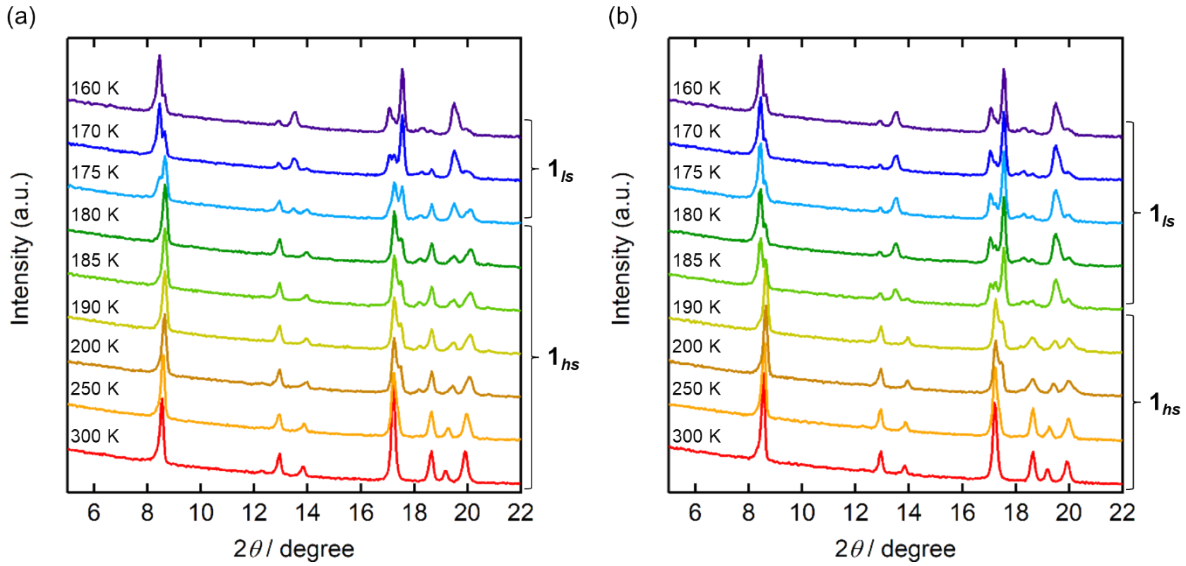

Figure S4. Variable temperature PXRD measurement of framework **1** under He in the temperature range of 160-300 K in the (a) cooling and (b) heating process. To avoid the influence of diffraction peaks from ice adhering to the capillary, only the region below 22° is shown.

Gas adsorption measurements

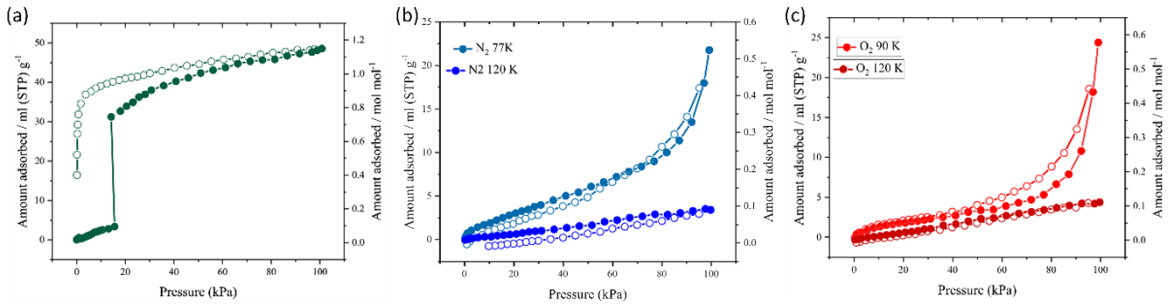

Figure S5. Adsorption isotherm of framework **1** under different adsorbent gases (a) CO_2 at 195 K, (b) N_2 at 77 K and 120 K, and (c) O_2 at 90 K and 120 K, respectively. Closed and Open circles correspond to desorption and adsorption, respectively.

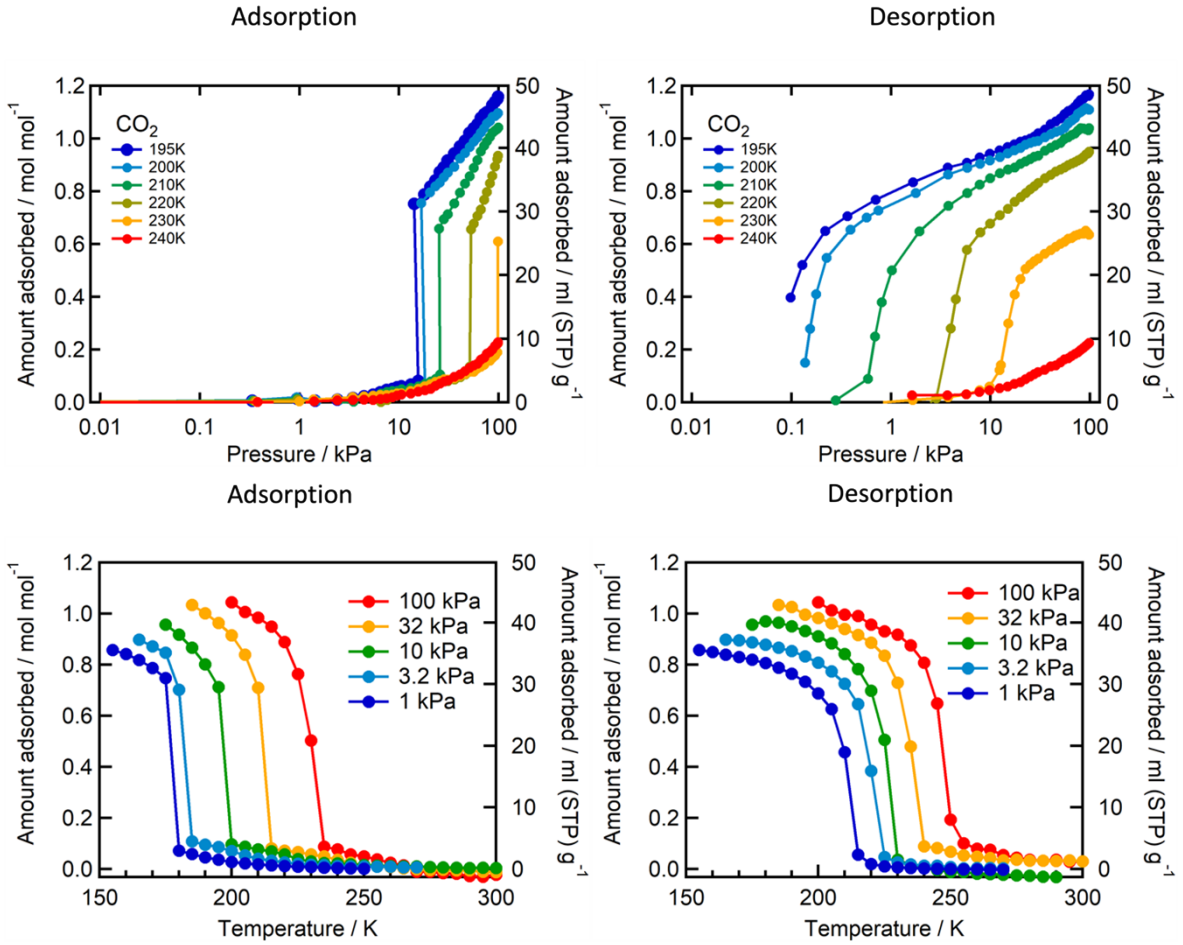

Figure S6. (top) CO_2 adsorption isotherms and (bottom) isobars of framework **1** at different temperatures and CO_2 pressures, respectively. Solid lines are only a guide for the eye.

Temperature dependence of the gated sorption pressure

The relationship between the GO/GC pressure and temperature was investigated in ln (*P*) vs. T^{-1} plots based on the Clausius-Clapeyron equation

$$\frac{d(lnP)}{dT^{-1}} = \frac{\Delta H_{trans}}{R_g} \qquad \text{---- Eq 1}$$

Where ΔH_{trans} is the transition enthalpy and R is the universal gas constant. Notably, the Clausius-Clapeyron equation is valid under an equilibrium condition, and hence it might not be suitable for applying to the present hysteretic behaviour. However, it was also theoretically revealed that the ln P vs. T^{-1} plots have a linear correlation even in the system showing hysteretic transition.[2]

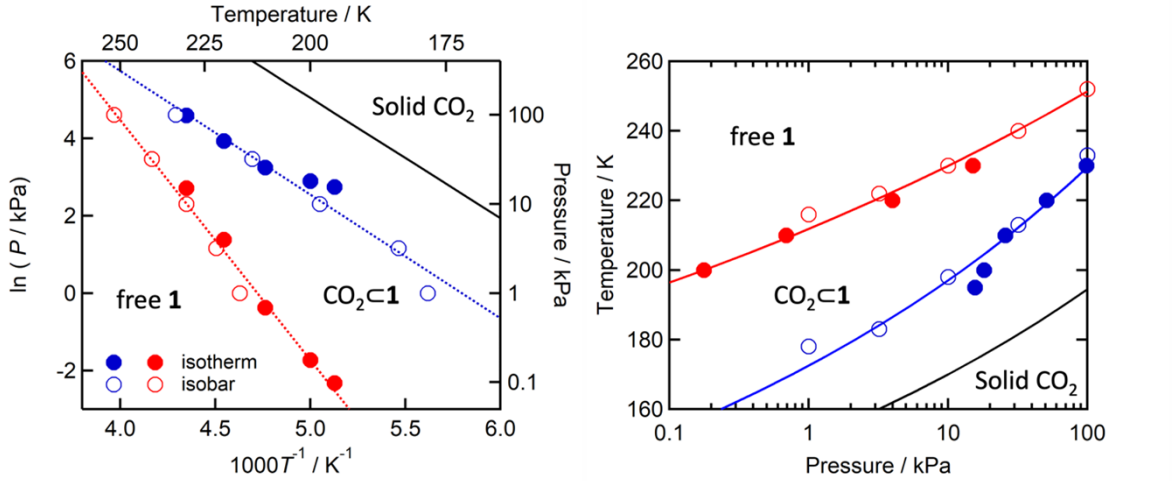

Figure S7. (left) Log-scale plots of the CO_2 pressure where GO (blue) and GC (red) occur *vs.* the inverse of the temperatures for GO/GC based on the CO_2 adsorption/desorption isotherms. The corresponding lines represent the fitting results based on the Clausius−Clapeyron equation 1. (right) Phase diagram for **1** and **1⊃CO₂ (1')**, where the blue and red lines represent the GO and GC, respectively, determined from CO_2 adsorption isotherms (closed circles) and isobars (open circles). The red and blue lines (right) represent the fitting based on the Clausius-Clapeyron equation (Eq 1). The black line represents the saturated vapour pressure curve, which distinguishes between the gas phase and the solid phase for bulk CO_2.

Determination of gate-opening/closing pressure under CO_2 ad/desorption at different temperatures

The gate opening (GO) and gate closing (GC) behaviours were observed in the CO_2 adsorption and desorption isotherms, respectively (Figure S6). The GO (or GC) pressures were determined as the peaks in dA_{ads}/dP plots from adsorption (or desorption) isotherms, where A_{ads} represents the amount adsorbed.

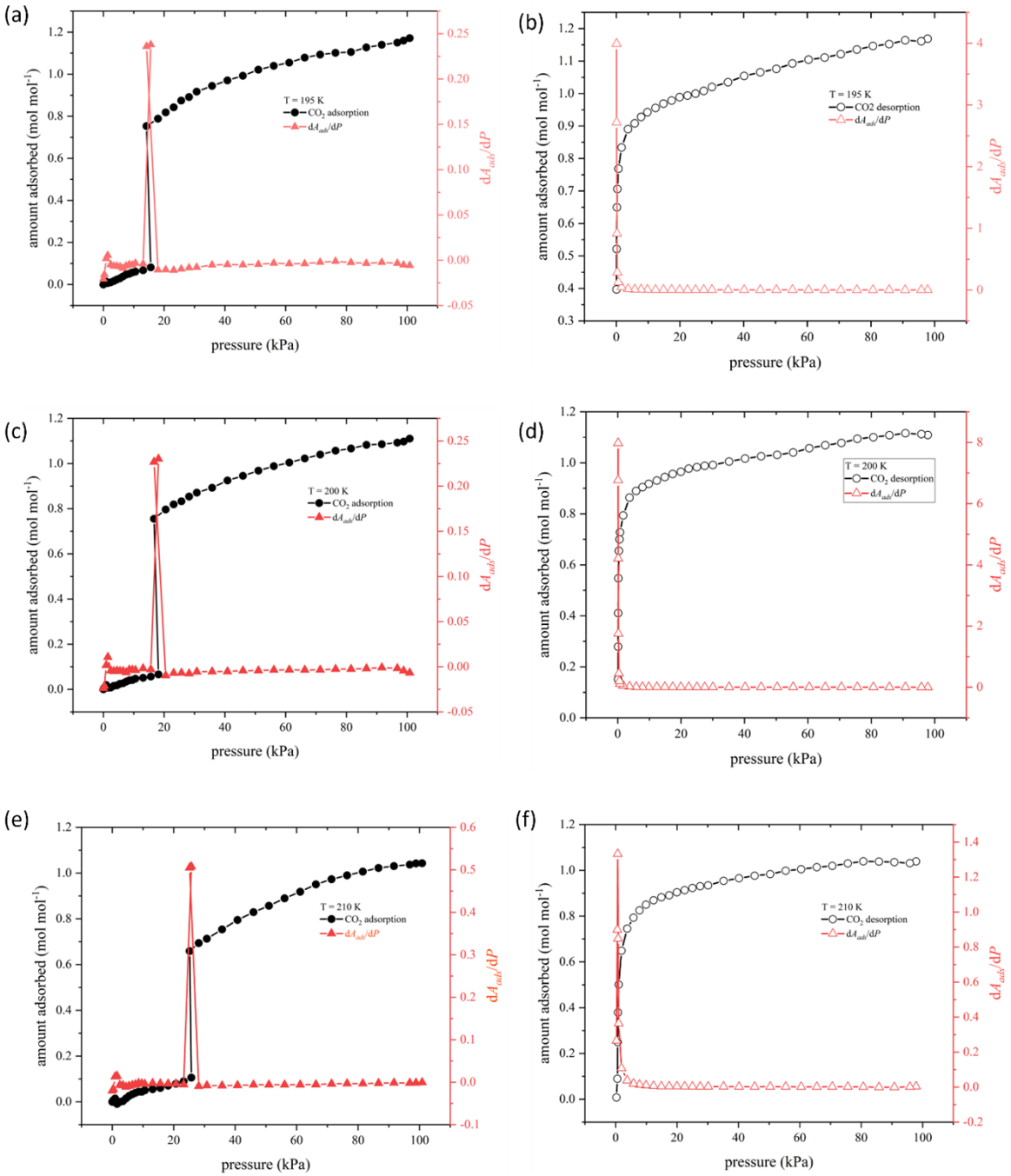

Figure S8. CO_2 adsorption (a, c, e) and desorption (b, d, f) isotherms (black) and dA_{ads}/dP *vs.* P plots (red) at 195 K (a, b), 200 K (c, d) and 210 K (e, f).

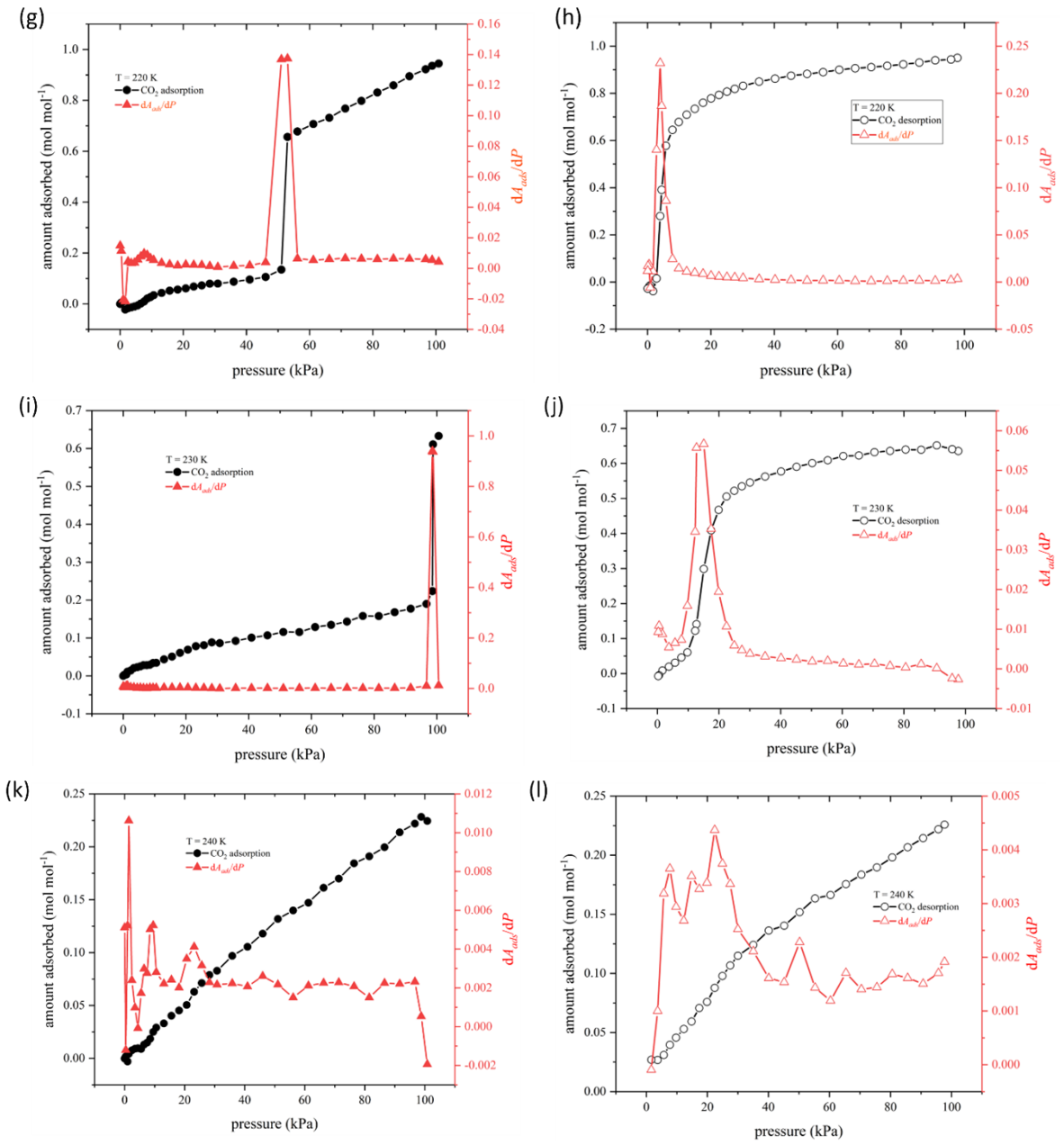

Figure S8 (continued). CO_2 adsorption (g, i, k) and desorption (h, j, l) isotherms (black) and dA_{ads}/dP *vs. P* plots (red) at 220 K (g, h), 230 K (i, j) and 240 K (k, l).

Determination of gate-opening/closing pressure under CO_2 ad/desorption at different pressures

The gate opening (GO) and gate closing (GC) behaviours were observed in the CO_2 adsorption and desorption isobars, respectively (Figure S6). The GO (or GC) pressures were determined as the peaks in dA_{ads}/dT plots from adsorption (or desorption) isobars, where A_{ads} represents the amount adsorbed.

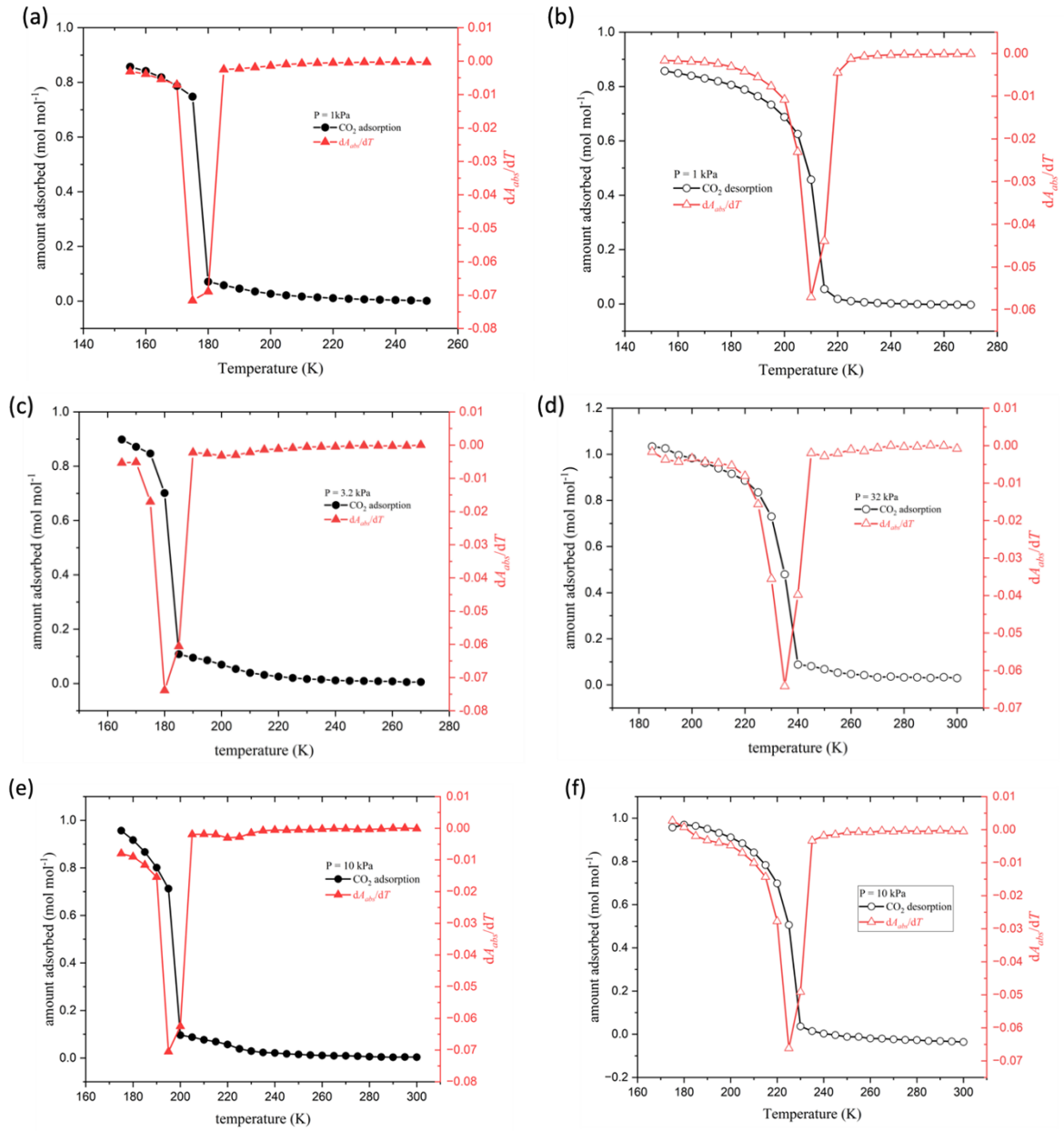

Figure S9. CO_2 adsorption (a, c, e) and desorption (b, d, f) isobars (black) and dA_{ads}/dT *vs.* T plots (red) at 1 kPa (a, b), 3.2 kPa (c, d) and 10 kPa (e, f).

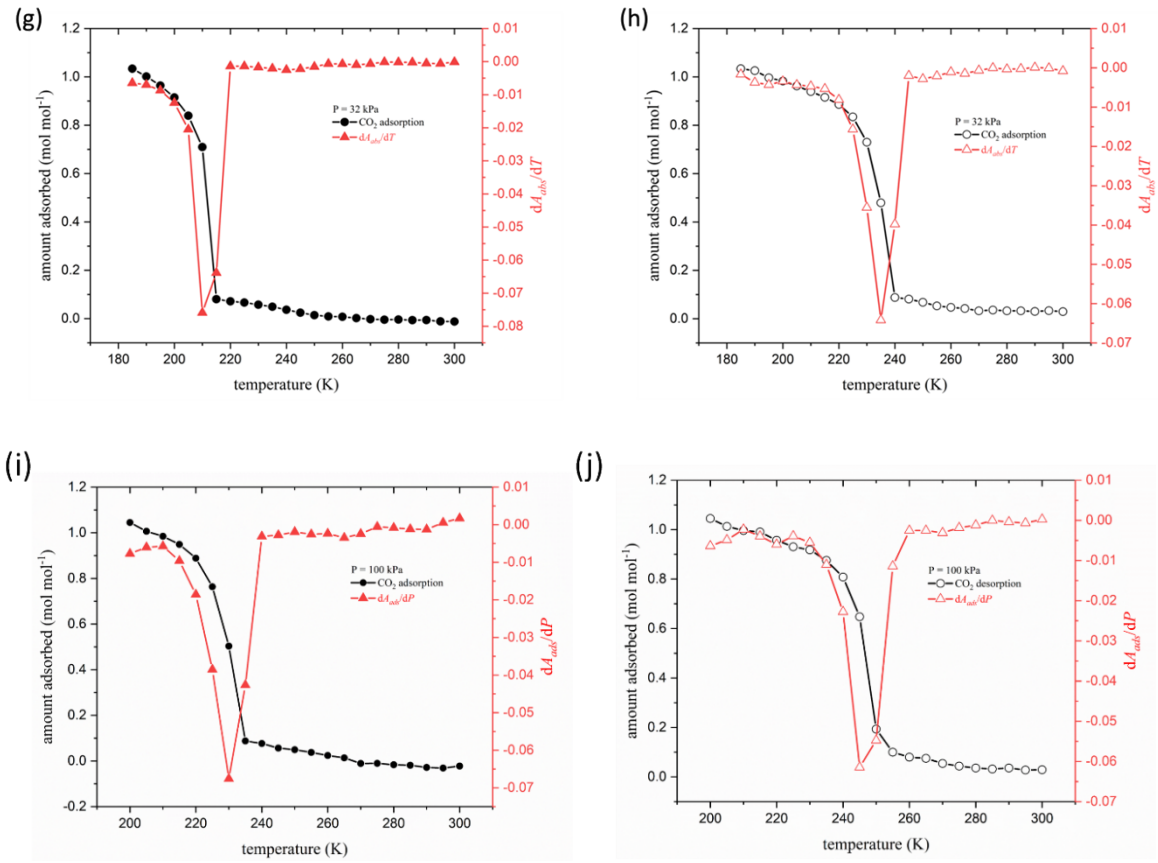

Figure S9 (continued). CO_2 adsorption (g, i) and desorption (h, j) isobars (black) and dA_{ads}/dT *vs. T* plots (red) at 32 kPa (g, h) and 100 kPa (i, j).

SCO transition for framework 1 at different CO_2 pressures.

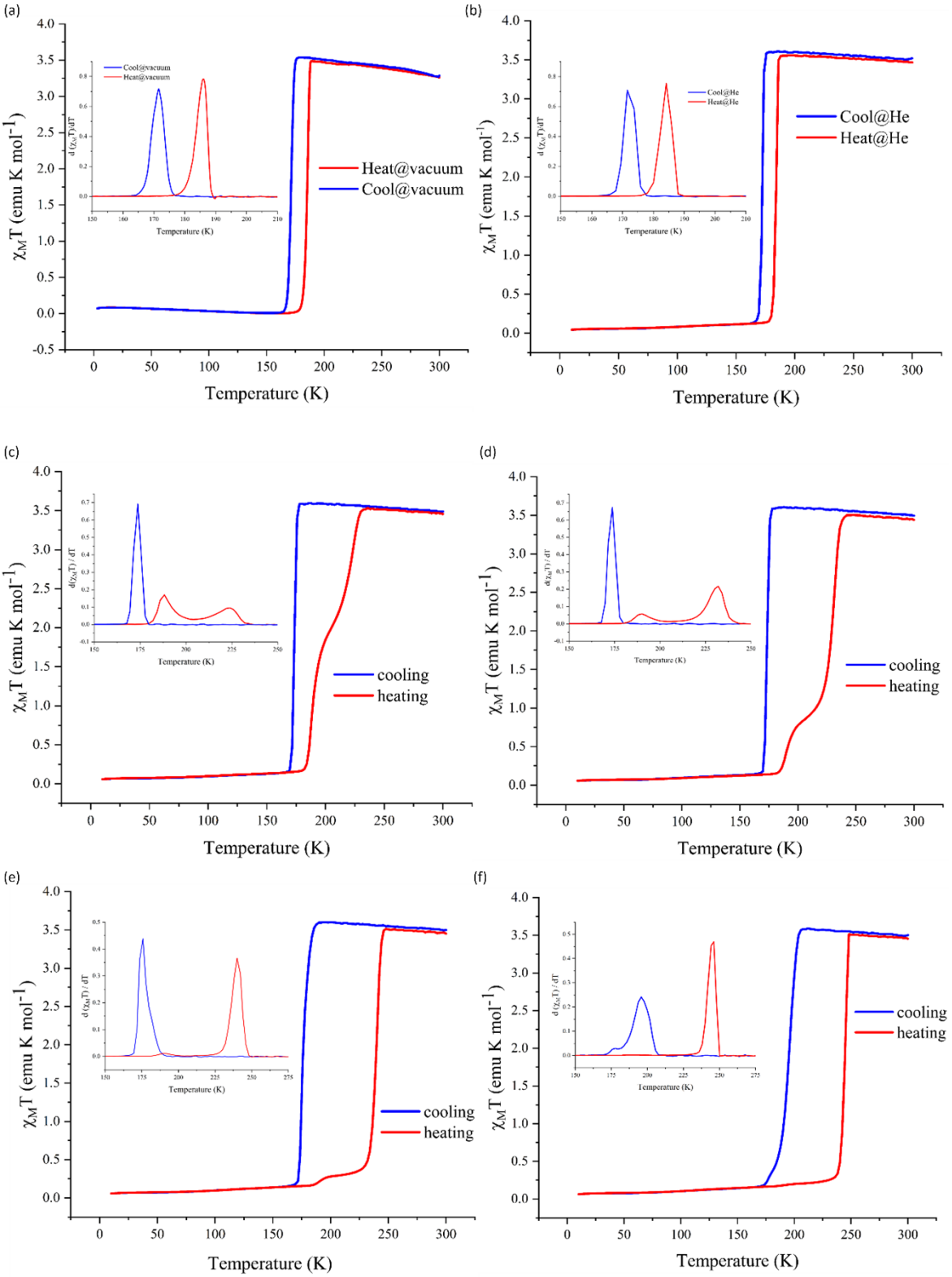

Figure S 10. Complete SCO transition for framework **1** in the temperature range of 10-300 K under an external magnetic field (H_{dc} = 1.0 kOe) at different conditions. (a) in absence of any gas (vacuum); (b) under 100 kPa He; (c) under P_{CO2} = 1.0 kPa; (d) P_{CO2} = 3.2 kPa; (e) under P_{CO2} = 10.0 kPa; (f) P_{CO2} = 32.0 kPa. (inset) transition temperatures as determined from the dc_MT/dT plot.

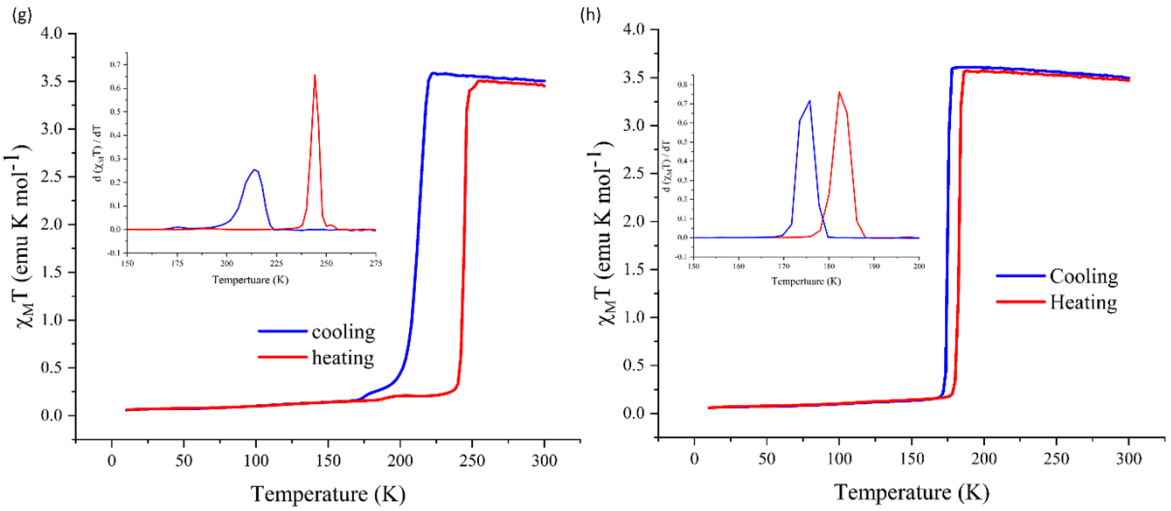

Figure S10 (continued). Complete SCO transition for framework **1** in the temperature range of 10-300 K under an external magnetic field (H_{dc} = 1.0 kOe) at (g) P_{CO2} = 100 kPa; (h) P_{CO2} = 0 kPa, 100 kPa He (repeated). (inset) transition temperatures as determined from the $d\chi_M T/dT$ plot.

Table S1. SCO transition temperatures[a] for framework 1 at different CO_2 pressure.

CO_2 Pressure (kPa)	T_{H1}	T_{H2}	T_C	δT (T_{H1}-T_C)	δT (T_{H2}-T_C)
0[b]	185	--	171	14	--
0[c]	186	--	171	15	--
1.0	188	224	173	15	51
3.2	190	232	173	17	59
10	190	240	175	15	65
32	--	246	195	51	--
100	--	245	213	32	--

[a]The transition temperatures were determined by the peaks at $d\chi_M T/dT$ vs. T plots.

[b]As P_{CO2} = 0 kPa, P_{He} = 100 kPa was filled in the gas cell instead of vacuum.

[c]As P_{CO2} = 0 kPa, magnetic measurements were performed under vacuum.

Determination of the CO_2-admixed states of framework 1 at different CO_2 pressures

From the magnetic characterisation under varied CO_2 pressure, it is evident that the CO_2 admixed states stabilize the LS states. Thus, the % of CO_2 admixed states present at different P_{CO2} was determined by the following equations.

$$\gamma_{HS} = \frac{(\chi_M T)_P - (\chi_M T)_{100}}{(\chi_M T)_{He} - (\chi_M T)_{100}} \quad \text{---- Eq 2}$$

$$\% \text{ of } \mathbf{1'} = 100 \times (1-\gamma_{HS}) \quad \text{---- Eq 3}$$

Where, γ_{HS} represents the residual HS fraction under consecutive P_{CO2}, $(\chi_M T)_P$, $(\chi_M T)_{100}$, and $(\chi_M T)_{He}$, represents the magnetic susceptibility values of framework **1** at the consecutive $P_{CO2,}$ 100 kPa CO_2 pressure and 100 kPa He pressure, respectively.

Table S2. determination of CO_2 admixed states of framework 1 at different CO_2 pressures

temperature	**190 K**	**196 K**	**200 K**	**206 K**
pressure	**1.0 kPa**	**3.2 kPa**	**10 kPa**	**32 kPa**
χMT of **1** under 100 kPa He	3.55	3.55	3.55	3.55
χMT of **1** under respective CO_2 pressure	1.14178	0.69157	0.28053	0.20539
χMT of **1** under 100 kPa CO_2	0.18509	0.20276	0.20844	0.20939
% of **1** in HS	28.411	14.57	2.154	0.12
Ratio of **1** in LS(%)	71.589	85.43	97.846	99.88

temperature	210 K	216 K	220 K	226 K
pressure	**1.0 kPa**	**3.2 kPa**	**10 kPa**	**32 kPa**
χMT of **1** under 100 kPa He	3.55	3.55	3.55	3.55
χMT of **1** under respective CO_2 pressure	2.1561	0.90641	0.29933	210.054
χMT of **1** under 100 kPa CO_2	0.20743	0.20616	0.20806	0.21714
% of **1** in HS	58.243	24.235	3.692	0.584
Ratio of **1** in LS(%)	41.757	75.765	96.308	99.416

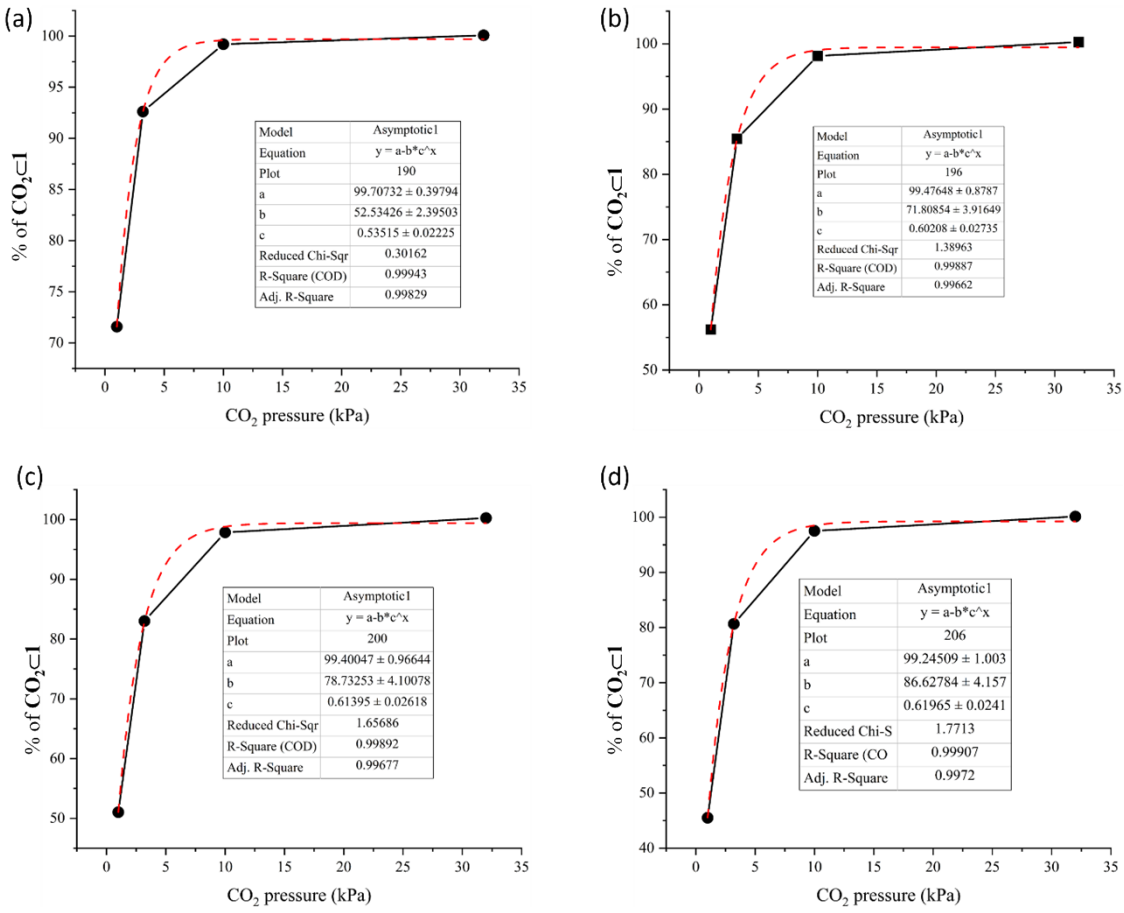

Figure S 11. Determination of the CO_2-admixed states of **1** at (a) 190 K, (b) 196 K, (c) 200 K and (d) 206 K. Red dashed line indicates the exponential fit.

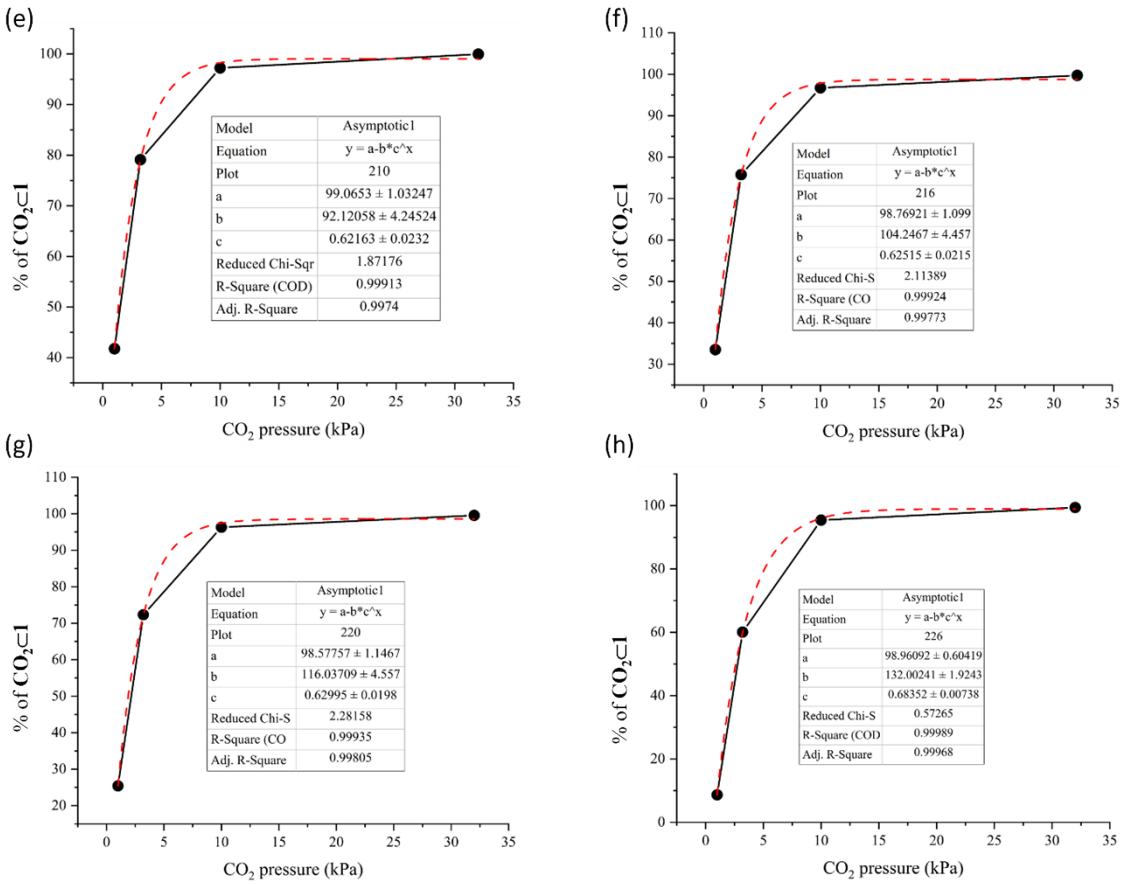

Figure S11 (continued). Determination of the CO_2-admixed states of **1** at (a) 210 K, (b) 216 K, (c) 220 K and (d) 226 K. Red dashed line indicates the exponential fit.

In situ VT-PXRD of framework 1 under CO_2

In situ variable-temperature (VT)-PXRD measurements were conducted to investigate the relationship between SCO and gated CO_2 adsorption in detail. For all conditions, measurements began at 260 K at fixed CO_2 pressure.

Figure S12a shows the PXRD pattern under 100 kPa of CO_2. Upon cooling, the PXRD pattern changed abruptly at around 225 K, which agrees with the temperature where gated CO_2 adsorption begins (Figure 3c). Since the PXRD pattern below 220 K was different from that of $\mathbf{1}_{ls}$ (Figure S4), the observed patterns are assigned to that of $\mathbf{1'}_{ls}$. In the present experiment, no intermediate phase was observed between $\mathbf{1}_{hs}$ and $\mathbf{1'}_{ls}$ in the cooling process, indicating that SCO was closely associated with the gated CO_2 adsorption. These results agree with the scheme shown in Figure 6b ($\mathbf{1}_{hs} \rightarrow \mathbf{1'}_{ls}$). Whereas, upon heating, the abrupt peak change was firstly observed at 245 K, then 255 K, which agrees with the temperatures of SCO (Figure 4c) and gated CO_2 desorption (Figure 3c), respectively. The pattern at 260 K was the same as the initial state, *i.e.*, $\mathbf{1}_{hs}$. Consequently, the PXRD pattern at 250 K was assigned to $\mathbf{1'}_{hs}$. These results agree with the scheme of the two-step phase transition shown in Figure 6d ($\mathbf{1'}_{ls} \rightarrow \mathbf{1'}_{hs} \rightarrow \mathbf{1}_{hs}$). These results also indicate that all four states, *i.e.*, $\mathbf{1}_{hs}$, $\mathbf{1}_{ls}$, $\mathbf{1'}_{hs}$, and $\mathbf{1'}_{ls}$, are distinguishable in PXRD patterns.

Figure S12b shows the PXRD pattern under 32 kPa of CO_2. Upon cooling, the PXRD pattern changed abruptly at around 205 K, which agrees with the temperature where gated CO_2 adsorption begins (Figure 3c). This indicates the occurrence of SCO associated with gated CO_2 adsorption ($\mathbf{1}_{hs} \rightarrow \mathbf{1'}_{ls}$). Upon heating, the abrupt peak change was observed at 245 K, which agrees with the temperatures of both SCO (Figure 4c) and gated CO_2 desorption (Figure 3c). Thus, PXRD patterns changed from $\mathbf{1'}_{ls}$ to $\mathbf{1}_{hs}$; different from PXRD under 100 kPa of CO_2, $\mathbf{1'}_{hs}$ was not observed.

Figure S12c and d show the PXRD pattern under 10 and 3.2 kPa of CO_2, respectively. Upon cooling, the change of PXRD pattern was recognised at around 180 K. Judging from the PXRD pattern, the patterns below 180 K contain both $\mathbf{1}_{ls}$ and $\mathbf{1'}_{ls}$. This indicates the occurrence of both temperature-induced SCO ($\mathbf{1}_{hs} \rightarrow \mathbf{1}_{ls}$) and CO_2-adsorption-induced SCO ($\mathbf{1}_{hs} \rightarrow \mathbf{1'}_{ls}$), which qualitatively agrees with the scheme shown in Figure 6a. Upon heating, the change of the PXRD pattern was recognised at around 190 K, which agrees with the SCO temperature of **1**, *i.e.*, $\mathbf{1}_{ls} \rightarrow \mathbf{1}_{hs}$ (Figure 4c). Then, the second peak change was observed at 240 and 230 K for 10 and 3.2 kPa of CO_2, respectively. These temperatures are slightly higher than gated CO_2 desorption temperature (Figure 3c), though they almost agree with SCO temperature at each CO_2 pressure (Figure 4c). Thus, the second peak shift can be ascribed to $\mathbf{1'}_{ls} \rightarrow \mathbf{1}_{hs}$. Totally in the heating process, a two-step transition involving phase mixing was observed ($\mathbf{1}_{ls} + \mathbf{1'}_{ls} \rightarrow \mathbf{1}_{hs} + \mathbf{1'}_{ls} \rightarrow \mathbf{1}_{hs}$), which qualitatively agrees with the scheme shown in Figure 6c.

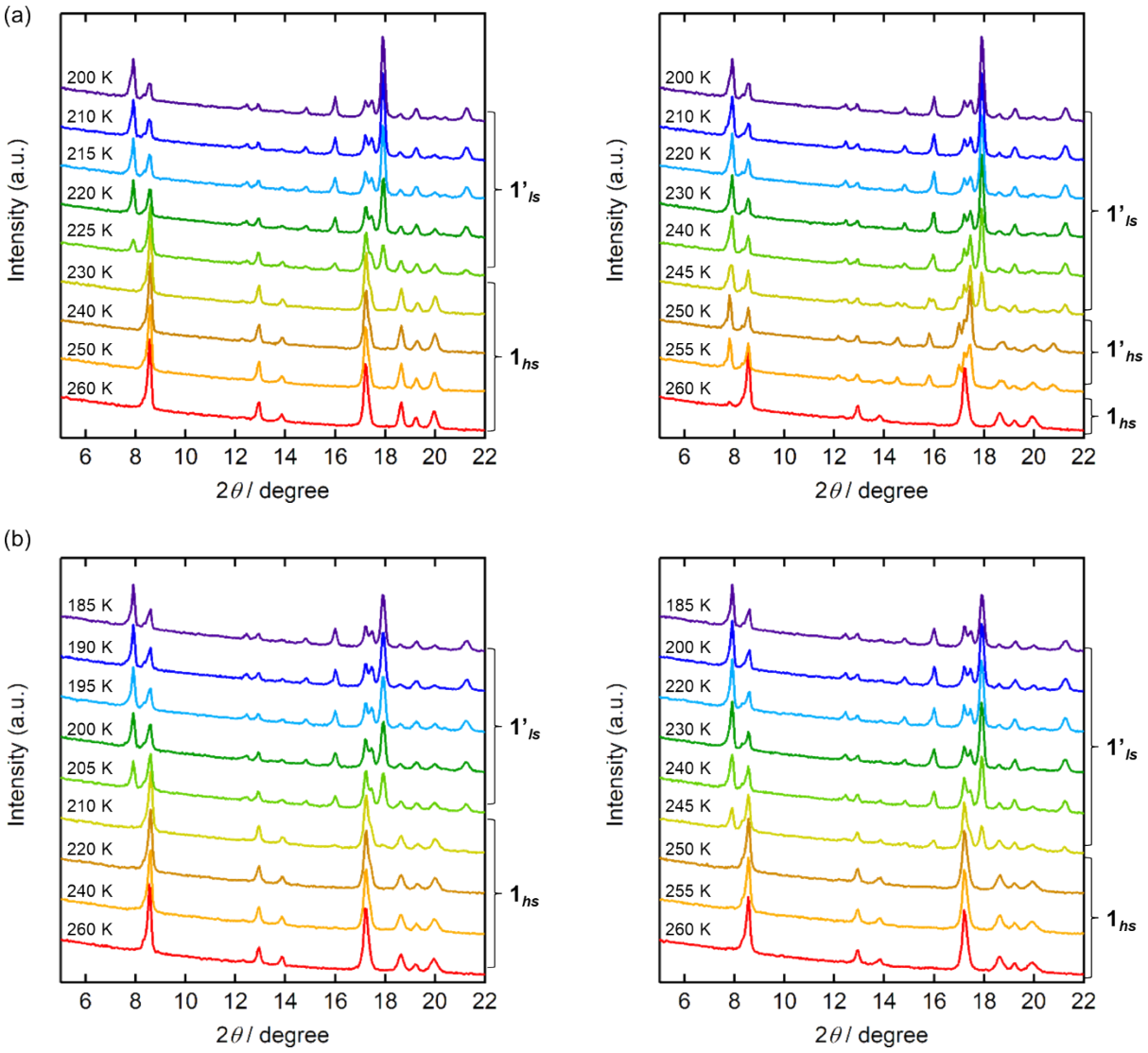

Figure S12. Variable temperature PXRD measurement of framework **1** under (a) 100 and (b) 32 kPa of CO_2 while cooling (left) and heating (right). To avoid the influence of diffraction peaks from ice adhering to the capillary, only the region below 22° is shown.

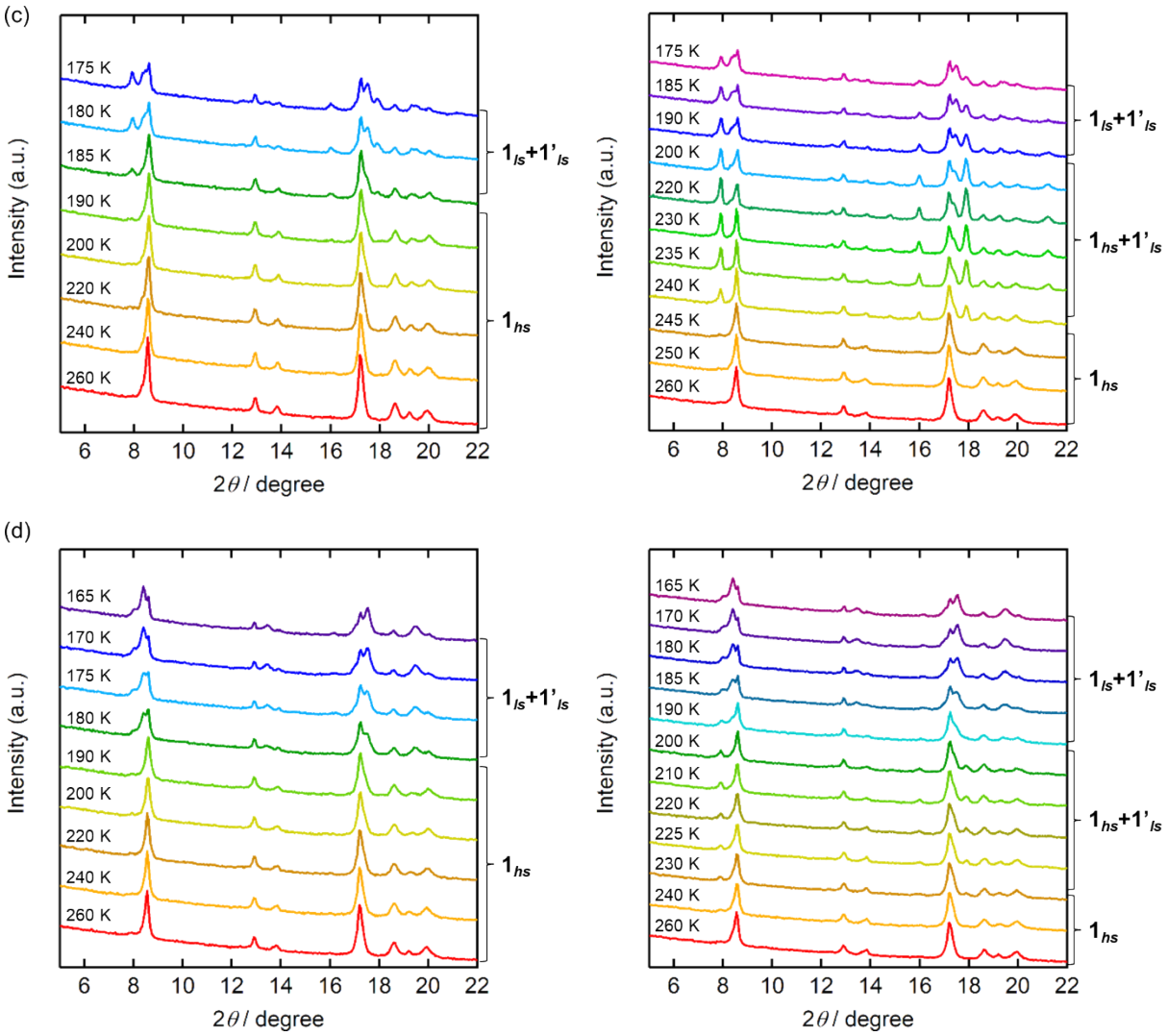

Figure S12 (Continued). Variable temperature PXRD measurement of **1** under (c) 10 and (b) 3.2 kPa of CO_2 while cooling (left) and heating (right). To avoid the influence of diffraction peaks from ice adhering to the capillary, only the region below 22° is shown.

Crystallographic details of $1 \cdot CS_2$

Table S3. Crystallographic data for $\mathbf{1 \cdot CS_2}$

Empirical formula	$C_{38}H_{28}Fe_2N_{12}O_8Pd_2S_4$
Formula weight	1233.46
Temperature/K	293(2)
Crystal system	monoclinic
Space group	I2/c
a/Å	7.3750(7)
b/Å	21.731(2)
c/Å	14.3104(13)
α/°	90
β/°	90.310(3)
γ/°	90
Volume/Å^3	2293.4(4)
Z	2
ρ_{calc}g/cm^3	1.786
μ/mm^{-1}	1.638
F(000)	1224.0
Radiation	MoKα (λ = 0.71073)
2Θ range for data collection/°	5.834 to 49.564
Index ranges	$-8 \leq h \leq 8$, $-25 \leq k \leq 25$, $-16 \leq l \leq 16$
Reflections collected	31892
Independent reflections	1897 [R_{int} = 0.0356, R_{sigma} = 0.0140]
Data/restraints/parameters	1897/0/144
Goodness-of-fit on F^2	1.186
Final R indexes [I>=2σ (I)]	R_1 = 0.0466, wR_2 = 0.1223
Final R indexes [all data]	R_1 = 0.0468, wR_2 = 0.1225
Largest diff. peak/hole / e Å^{-3}	1.18/-0.60

Table S4. Selected bond lengths for $\mathbf{1 \cdot CS_2}$

Atom	Atom	Length/Å	Atom	Atom	Length/Å
Pd01	C008	1.988(6)	O00G	C00N	1.208(9)
Pd01	C008[1]	1.988(6)	N004	C009	1.155(8)
Pd01	C009[2]	1.980(6)	N005	C008	1.155(8)
Pd01	C009[3]	1.980(6)	N00C	C00I	1.340(8)
Fe02	N004[4]	2.030(5)	N00C	C00K	1.344(8)
Fe02	N004	2.030(5)	C00I	C00L	1.380(9)
Fe02	N005	2.041(5)	C00K	C00Q	1.376(10)
Fe02	N005[4]	2.041(5)	C00L	C00O	1.388(9)
Fe02	N00C	2.117(5)	C00N	C00O	1.493(10)
Fe02	N00C[4]	2.117(5)	C00O	C00Q	1.391(10)
O00D	C00N	1.342(8)	S1	C3	1.468(18)
O00D	C00U	1.449(8)			

[1]1-X,+Y,1/2-Z; [2]-X,+Y,1/2-Z; [3]1+X,+Y,+Z; [4]-X,-Y,1-Z

Table S5. Selected bond angles for **1·CS$_2$**

C008	Pd01	C008[1]	176.7(3)	N00C	Fe02	N00C[4]	180.0
C009[2]	Pd01	C008[1]	91.4(2)	C00N	O00D	C00U	115.0(5)
C009[3]	Pd01	C008	91.4(2)	C009	N004	Fe02	172.7(4)
C009[3]	Pd01	C008[1]	88.6(2)	C008	N005	Fe02	174.9(4)
C009[2]	Pd01	C008	88.6(2)	C00I	N00C	Fe02	120.2(4)
C009[2]	Pd01	C009[3]	178.7(3)	C00I	N00C	C00K	116.3(6)
N004	Fe02	N004[4]	180.0(2)	C00K	N00C	Fe02	123.1(4)
N004	Fe02	N005	89.81(18)	N005	C008	Pd01	176.1(5)
N004[4]	Fe02	N005	90.19(18)	N004	C009	Pd01[5]	176.3(5)
N004	Fe02	N005[4]	90.19(18)	N00C	C00I	C00L	123.9(6)
N004[4]	Fe02	N005[4]	89.81(18)	N00C	C00K	C00Q	124.1(6)
N004[4]	Fe02	N00C	89.11(18)	C00I	C00L	C00O	118.5(6)
N004	Fe02	N00C	90.89(18)	O00D	C00N	C00O	111.3(6)
N004	Fe02	N00C[4]	89.11(18)	O00G	C00N	O00D	124.2(7)
N004[4]	Fe02	N00C[4]	90.89(18)	O00G	C00N	C00O	124.5(6)
N005	Fe02	N005[4]	180.0	C00L	C00O	C00N	123.3(6)
N005	Fe02	N00C	88.76(18)	C00L	C00O	C00Q	118.5(6)
N005	Fe02	N00C[4]	91.24(18)	C00Q	C00O	C00N	118.3(6)
N005[4]	Fe02	N00C	91.24(18)	C00K	C00Q	C00O	118.5(6)
N005[4]	Fe02	N00C[4]	88.76(18)	S1[6]	C3	S1	180.0

[1]1-X,+Y,1/2-Z; [2]-X,+Y,1/2-Z; [3]1+X,+Y,+Z; [4]-X,-Y,1-Z; [5]-1+X,+Y,+Z; [6]1/2-X,1/2-Y,1/2-Z

Table S6. Torsional angles for **1·CS$_2$**

A	B	C	D	Angle/°	A	B	C	D	Angle/°
Fe02	N00C	C00I	C00L	179.2(5)	C00I	N00C	C00K	C00Q	-2.4(9)
Fe02	N00C	C00K	C00Q	175.1(5)	C00I	C00L	C00O	C00N	178.8(6)
O00D	C00N	C00O	C00L	11.9(9)	C00I	C00L	C00O	C00Q	-2.7(9)
O00D	C00N	C00O	C00Q	-166.6(6)	C00K	N00C	C00I	C00L	-6.2(9)
O00G	C00N	C00O	C00L	-168.9(7)	C00L	C00O	C00Q	C00K	-0.8(9)
O00G	C00N	C00O	C00Q	12.6(10)	C00N	C00O	C00Q	C00K	177.8(6)
N00C	C00I	C00L	C00O	6.5(9)	C00U	O00D	C00N	O00G	-1.2(9)
N00C	C00K	C00Q	C00O	1.0(10)	C00U	O00D	C00N	C00O	178.0(5)

Structural diagram for $1{\cdot}CS_2$

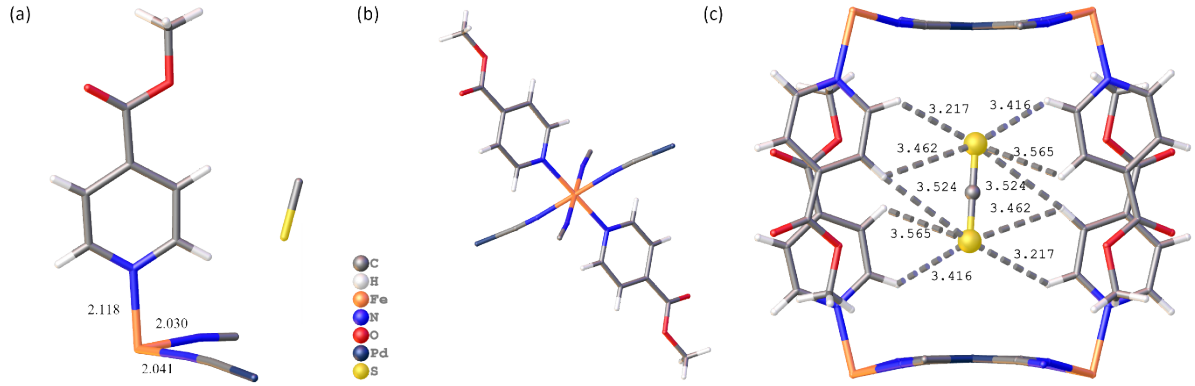

Figure S13. (a) Asymmetric unit of **1·CS$_2$**, indicating Fe-N bond lengths; (b) a single [FeN$_6$] unit of **1·CS$_2$** framework; (c) S···Pd short contacts and the array of C-H···S bonding stabilizing the CS_2 molecule inside the framework channel. Color code: grey, C; red, O; blue, N; yellow, S; orange, Fe; navy, Pd.

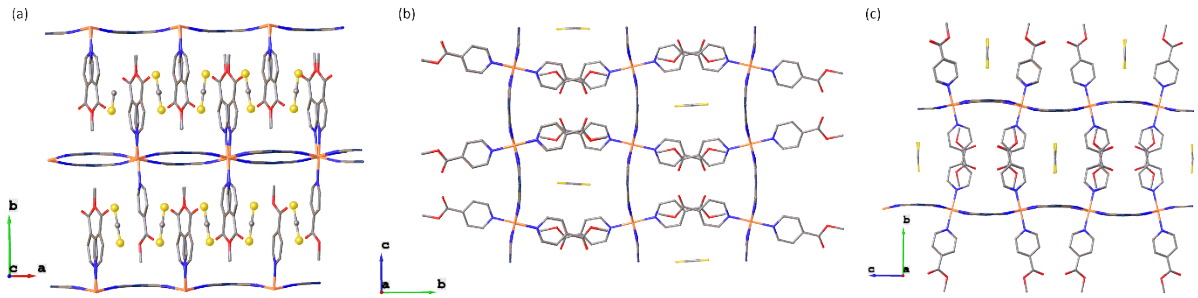

Figure S 14. Molecular packing diagram of **1**·CS_2 along crystallographic axes *a*, *b* and *c*, respectively.

References in ESI

1. Mondal, D. J.; Mondal, A.; Paul, A.; Konar, S., Guest-Induced Multistep-to-One-Step Reversible Spin Transition with Enhanced Hysteresis in a 2D Hofmann Framework. *Inorg. Chem.* **2022,** *61* (11), 4572-4580.
2. Numaguchi, R.; Tanaka, H.; Watanabe, S.; Miyahara, M. T., Simulation study for adsorption-induced structural transition in stacked-layer porous coordination polymers: Equilibrium and hysteretic adsorption behaviors. *J. Chem. Phys.* **2013,** *138* (5).